Electrochimica Acta 60 (2012) 55–65

Contents lists available at SciVerse ScienceDirect

Electrochimica Acta

journal homepage: www.elsevier.com/locate/electacta

A study of the agglomerate catalyst layer for the cathode side of a proton exchange membrane fuel cell: Modeling and optimization

N. Khajeh-Hosseini-Dalasm[a,*], M. Fesanghary[b], K. Fushinobu[a], K. Okazaki[a]

[a] Department of Mechanical and Control Engineering, Tokyo Institute of Technology, Meguro-ku, Tokyo 152-8552, Japan
[b] Department of Mechanical Engineering, Louisiana State University, 2508 Patrick Taylor Hall, Baton Rouge, LA 70803, United States

ARTICLE INFO

Article history:
Received 5 September 2011
Received in revised form 30 October 2011
Accepted 31 October 2011
Available online 23 November 2011

Keywords:
Catalyst layer
Structural parameters
Analysis of means
Analysis of variance
Optimization

ABSTRACT

A comprehensive mathematical model for the cathode catalyst layer (CL) of a proton exchange membrane fuel cell (PEMFC) is developed to investigate its performance, which is determined by activation overpotential. Numerous cathode CL parameters such as the saturation and eight structural parameters, namely, ionomer film thickness covering each agglomerate, agglomerate radius, platinum loading, carbon loading, ionomer volume fraction, gas diffusion layer penetration content and its porosity, and CL thickness are taken into account. The main effects of each parameter and their interactions are investigated using the analysis of means (ANOM) and interaction plots, respectively. Analysis of variance (ANOVA) is used to identify the influence of the CL structural parameters on the activation overpotential. Finally, an evolutionary optimization algorithm is employed to maximize the cathode CL's performance.

© 2011 Elsevier Ltd. All rights reserved.

1. Introduction

Over the past two decades, proton exchange membrane fuel cells (PEMFCs) have received attention due to increases in energy price and concerns about environmental pollution. Low pollutants emission, high energy conversion efficiency, and low operating temperature are characteristics of the fuel cells that are making this technology attractive. PEMFCs are considered to be among the most promising candidates for transportation, portable and stationary applications. The performance of PEMFCs is significantly affected by cathode catalyst layer's (CL) performance. In recent years numerous research works have been conducted to study the performance enhancement of cathode CL. Despite achievements in this area the CL losses due to reactant transport limitations and poor oxygen reduction reaction (ORR) kinetics have major contributions toward decreasing PEM fuel cell efficiency [1–3]. In order to enhance the CL performance and therefore increase the PEM fuel cell efficiency, it is important to realize the dependence of CL performance on its structural characteristics. In this study, a mathematical model of cathode CL, which takes numerous CL parameters into account, is developed and described. The interaction between the parameters (factors) and their relative importance is investigated. Finally, optimization is performed to find the best CL performance.

Cathode CL models can be broadly classified into three different categories based on their level of complexity: interface models, macro-homogeneous models, and agglomerate models. Interface models simply treat the CL as an infinitely thin layer. As a result spatial variations within the CL are ignored and different phase potentials are not considered. In these models exchange current densities are usually modified to match experimental data and cell current density is always over estimated. A macro-homogeneous model can consider different phase potentials [4–6]. However, it cannot assess the complex multi-material structure of the CL. Unlike interface and macro-homogeneous models, the composition and structural distribution of CL materials are taken into account in agglomerate models. Agglomerate models results agree with experimental observations which showed that a CL is composed of the agglomeration of catalyst particles (platinum and carbon) and an ionomer [7–9].

Beginning with the pioneering work of Ridge et al. [10] many other agglomerate models have been developed especially in recent years. Several parametric studies have been conducted to investigate the dependency of CL performance on CL structural and operational parameters. Wang et al. [11] studied the performance of two different types of spherical agglomerates: (1) filled with proton conduction ionomer; (2) filled with liquid water. They showed that water-filled agglomerates can have a larger effectiveness factor if the cathode transfer function is close to 1. In addition, the influence of the agglomerate radius on CL performance indicated that there should be an optimum value for the agglomerate radius. Sun et al. [12] employed a two-dimensional ionomer-filled spherical

* Corresponding author. Tel.: +81 3 5734 2179; fax: +81 3 5734 2179.
E-mail address: navvabk@yahoo.com (N. Khajeh-Hosseini-Dalasm).

0013-4686/$ – see front matter © 2011 Elsevier Ltd. All rights reserved.
doi:10.1016/j.electacta.2011.10.099

Nomenclature

a	active surface area within the agglomerate, m^{-1}
a_{agg}	total external area of active sites of agglomerate per unite volume of CL, m^{-1}
A	total active area of agglomerate per unite volume of CL, m^{-1}
A_s	reaction surface area per unite mass of platinum, $m^2\ kg^{-1}$
c	concentration, $mol\ m^{-3}$
d_{avg}	average pore diameter, m
D_{O_2}	diffusion coefficient, $m^2\ s^{-1}$
D_{Kn}	Knudsen diffusion coefficient, $m^2\ s^{-1}$
E	effectiveness factor
f	mass fraction of platinum to that of Pt/C particles
F	Faraday constant, 96,485 coulombs mol^{-1}
i	local current density, $A\ m^{-2}$
i_0	exchange current density, $A\ m^{-2}$
I_δ	cell current density, $A\ m^{-2}$
k_l	reaction rate constant, $m\ s^{-1}$
l_c	catalyst layer thickness, m
$L_{g,c}$	volume fraction of GDL penetrating into the CL
$L_{m,c}$	volume fraction of ionomer phase in the CL
L_s	volume fraction of the GDL material penetrated into the CL
m_{Pt}	platinum mass loading, $kg\ m^{-2}$
m_C	carbon mass loading, $kg\ m^{-2}$
M	molecular weight, $kg\ mol^{-1}$
M_T	Thiele module
n_{agg}	number of agglomerates per unite volume of CL, m^{-3}
P	pressure, Pa
r_{agg}	agglomerate radius, m
R	dissolved oxygen molar rate per unit of agglomerates, $mol\ m^{-3}\ s^{-1}$
$\overline{R}$	universal gas constant, $8.314\ J\ mol^{-1}\ K^{-1}$
s	liquid water saturation
T	temperature, K
V	volume, m^3
r, z	coordinate, m

Greek letters

α	transfer coefficient
δ_{agg}	ionomer film thickness, m
ε_{agg}	ionomer volume fraction inside agglomerates
ε_c	CL porosity
ε_g	GDL porosity
η	activation overpotential, V
ρ_C	carbon density, $kg\ m^{-3}$
ρ_{Pt}	platinum density, $kg\ m^{-3}$
σ	electronic conductivity, $S\ m^{-1}$
κ	protonic conductivity, $S\ m^{-1}$
τ	CL tortuosity

agglomerate model to study the effects of ionomer volume fraction and platinum loading. It was predicted that there is an optimum level for the ionomer volume fraction. This conclusion was drawn from analyzing the effects of ionomer volume fraction on CL performance while other parameter levels (e.g., platinum loading) were kept constant. Possible interaction between (or dependence on) CL ionomer volume fraction and platinum loading was experimentally examined by Sasikumar et al. [13] who concluded that the optimum ionomer volume fraction should depend on the platinum loading. This was numerically confirmed in Yin's [14] work, in which two different types of agglomerates were compared: (1) agglomerate with platinum on its surface partially covered by an ionomer; (2) agglomerate with an ionomer film covering the agglomerate surfaces completely. A preliminary study was conducted to evaluate the dependency of current density on platinum and ionomer loadings, CL porosity, and CL thickness. However, Yin [14] ignored the presence of liquid water in open macro-pores between agglomerates and the penetration of GDL material into the CL. A parametric study on the effects of CL structural parameters including agglomerate radius and ionomer volume fraction was performed by Secanell et al. [15]. It was concluded that the CL performance increases monotonically with the reduction of the agglomerate radius. This conclusion was drawn without considering possible interactions between the agglomerate radius and other parameters, i.e., CL pore diameter, porosity, and tortuosity. Accordingly, Kamarajugadda and Mazumder [16] confirmed that there is an optimal performance with changing ionomer volume fraction. This is due to local agglomerate level mass transport and conductivity losses in the ionomer film thickness covering agglomerates. However, the presence of liquid water in open macro pores was neglected. The effect of liquid water was taken into account by Madhusudana Rao et al. [17] without inclusion of agglomerate geometrical properties and with an assumption that there is a uniform liquid water film covering each agglomerate surface.

Most of the papers mentioned above focused on analyzing the effect of one factor at a time. The main drawback of analyzing one factor at a time is that such an approach ignores the possible interactions between input (structural) factors. Two factors interact if the effects of one of the factors differs depending on the value of the other factor. More comprehensive models should be developed together with inclusive parametric studies in order to investigate possible interactions between the CL parameters.

In this study a comprehensive steady-state one-dimensional agglomerate model is developed. It takes into account (1) the effects of nine operational and structural parameters, namely, the saturation and eight catalyst layer structural parameters (ionomer film thickness covering each agglomerate, agglomerate radius, platinum loading, carbon loading, ionomer volume fraction, gas diffusion layer penetration content and its porosity, and CL thickness); (2) the material balance relationships in the CL; (3) the possible interactions between input parameters; (4) Knudsen diffusion when the open pore diameter is small and solid wall effect is important. Analysis of means (ANOM) and analysis of variance (ANOVA) are performed. They indicate the main effects and relative importance of input parameters, respectively. In addition, an evolutionary optimization method based on the harmony search algorithm (HS) is employed to optimize the CL parameters (i.e., minimize the CL activation overpotential) [25].

2. Catalyst layer mathematical model

In this study, a one-dimensional mathematical model which considers an agglomerate structure for the cathode catalyst layer is developed. Shown in Fig. 1 is a cathode CL as a layer which is sandwiched between the cathode GDL and membrane. The CL is composed of homogenous agglomerates. Each agglomerate is composed of an intermixed Nafion ionomer, and platinum and carbon particles. While secondary pores exist between the agglomerates allowing gas diffusion (i.e., oxygen gas diffusion), primary pores inside each agglomerate are filled with an ionomer phase and allow for (dissolved) oxygen diffusion and proton migration. The following parameters are introduced to define the structural characteristics of the CL

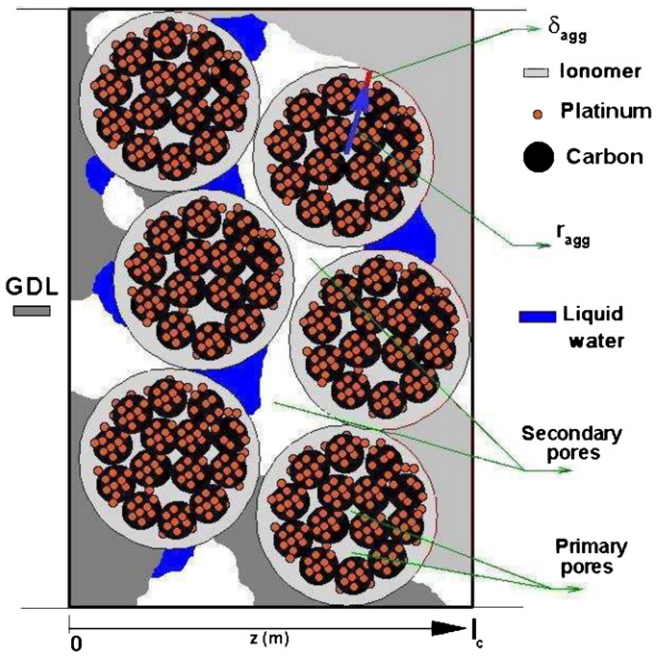

Fig. 1. Schematic representation of the agglomerate based cathode CL for a PEM fuel cell.

- Secondary pores may be partially or fully filled with liquid water. The volume fraction of the pores, which is filled with liquid water is called the liquid water saturation and is denoted by s.
- Each agglomerate has a radius r_{agg} and may be covered with an ionomer film of uniform thickness δ_{agg}.
- Platinum loading and carbon loading are denoted by m_{Pt} and m_C, respectively.
- The total volume fraction of the ionomer phase in the CL is $L_{m,c}$.
- The GDL material has porosity ε_g and may also partially penetrate in the CL. The penetration takes place due to compression during MEA assembly. GDL penetrated content is shown by $L_{g,c}$.
- The CL thickness is denoted by l_c.

The mathematical model describes and derives the equations for electrochemical reaction rate, diffusion of oxygen, and activation overpotential. Each of these equations is addressed separately (see below).

2.1. Electrochemical reaction rate

Molar conservation of dissolved oxygen inside a spherical agglomerate along the radial direction is expressed by

$$-\frac{1}{r^2}\left(\frac{d}{dr}r^2 N_{O_2,r}\right) + R_{O_2,r} = 0 \tag{1}$$

where $N_{O_2,r}$ shows radial molar flux of dissolved oxygen in the ionomer phase of an agglomerate. The dissolved oxygen molar consumption rate per unit volume, as a result of ORR, is denoted by R_{O_2}. Fick's diffusion law is used to relate the radial dissolved oxygen molar flux $N_{O_2,r}$ to a gradient of its concentration c_{O_2}

$$N_{O_2,r} = -D^{eff}_{O_2,m}\frac{dc_{O_2,r}}{dr} \tag{2}$$

where $D_{O_2,m}$ is the effective dissolved oxygen diffusion coefficient inside an agglomerate. The diffusion coefficient can be related to its bulk value $D_{O_2,m}$ as

$$D^{eff}_{O_2,m} = \varepsilon^{\tau}_{agg} D_{O_2,m} \tag{3}$$

where ε_{agg} is the volume fraction of the ionomer phase inside agglomerates. τ is tortuosity. The reaction rate R_{O_2} in Eq. (1) is first-order with respect to the dissolved oxygen concentration [18]

$$R_{O_2,r} = -k_1 a c_{O_2,r} \tag{4}$$

where a is the active surface area per unit volume within an agglomerate. A combination of Eqs. (1)–(4) leads to

$$\frac{D^{eff}_{O_2,m}}{r^2}\left(\frac{d}{dr}r^2\frac{dc_{O_2,r}}{dr}\right) - k_1 a c_{O_2,r} = 0 \tag{5}$$

Eq. (5) can be solved analytically by employing the following boundary conditions for a spherical agglomerate

$$\left.\frac{dc_{O_2,r}}{dr}\right|_{r=0} = 0 \tag{6}$$

$$c_{O_2,r}\big|_{r=r_{agg}} = c_{O_2,agg-film} \tag{7}$$

where $c_{O_2,agg-film}$ denotes the dissolved oxygen concentration at the interface of an agglomerate's core and the ionomer film covering the agglomerate. The solution can be expressed by an effectiveness factor E. The factor is a measure of how much the reaction rate reduces as a result of diffusion resistance. For the spherical geometry of an agglomerate and first order reaction [18]

$$E = \frac{\bar{c}_{O_2}}{c_{O_2,agg-film}} = \frac{1}{M_T}\left(\frac{1}{\tanh(3M_T)} - \frac{1}{3M_T}\right) \tag{8}$$

where $\bar{c}_{O_2}$ is the mean dissolved oxygen concentration within an agglomerate. In Eq. (8) Thiele module, M_T, is obtained as

$$M_T = \frac{r_{agg}}{3}\sqrt{\frac{k_1 a}{D^{eff}_{O_2,m}}} \tag{9}$$

An expression for a mean source term $\bar{R}_{O_2}$ versus the reaction order k_1 can be obtained using Eqs. (4) and (8)

$$\bar{R}_{O_2} = -k_1 a \bar{c}_{O_2} = -E k_1 a c_{O_2,agg-film} \tag{10}$$

In Eq. 9 a is the active reaction surface area per total volume of the agglomerates. Therefore, R_{O_2} is obtained for the total volume of the agglomerates. Following these derivations, a description of the dissolved oxygen concentration on the interface of the agglomerate's core and ionomer film $c_{O_2,agg-film}$ was sought. This can be done by taking the molar conservation of dissolved oxygen in the ionomer film into account. For the spherical shell of the ionomer film, δ_{agg}, covering each agglomerate, in which no reaction (no production or consumption of dissolved oxygen) takes place, the conservation equation is

$$\frac{d}{dr}\left(r^2 D_{O_2,m}\frac{dc_{O_2}}{dr}\right) = 0 \tag{11}$$

Dissolved oxygen flux should be continuous at the interface, i.e., $r = r_{agg}$, which gives

$$a_{agg} D_{O_2,m}\frac{r_{agg}}{r_{agg}+\delta_{agg}}\left(\frac{c_{O_2,film-pore} - c_{O_2,agg-film}}{\delta_{agg}}\right) = AEk_1 c_{O_2,agg-film} \tag{12}$$

where a_{agg} is the total external area of active sites of agglomerates per unit volume of the CL. A denotes the total active area of agglomerates per unit volume in the CL. In Eq. (12) the dissolved oxygen

concentration on the agglomerate surface (on the ionomer film and pores interface) is described by Henry's law for an equilibrium state

$$c_{O_2,\text{film-pore}} = \frac{c_{O_2}}{K_{O_2}} \tag{13}$$

where K_{O_2} is the dimensionless Henry's constant calculated from [19]

$$K_{O_2} = \frac{1}{RT}\exp\left(-\frac{666}{T} + 14.1\right) \tag{14}$$

Combining Eqs. (12) and (10), an expression for the source term R_{O_2} with respect to c_{O_2} is obtained as follows

$$c_{O_2,\text{agg-film}} = \left(1 + \frac{AEk_1\delta_{agg}}{a_{agg}D_{O_2,m}}\frac{r_{agg}+\delta_{agg}}{r_{agg}}\right)^{-1}\frac{c_{O_2}}{K_{O_2}} \tag{15}$$

$$R_{O_2} = -\left(\frac{1}{Ek_1a} + \frac{A}{a}\frac{\delta}{a_{agg}D_{O_2,m}}\frac{r_{agg}+\delta}{r_{agg}}\right)^{-1}\frac{c_{O_2}}{K_{O_2}} \tag{16}$$

The oxygen source term (consumption rate) per unit volume of the CL can be related to the protonic current density i as

$$R_{O_2}\frac{A}{a} = -\frac{1}{4F}\nabla\cdot i \tag{17}$$

In Eq. (17) R_{O_2} is multiplied by A/a to give an oxygen consumption rate per unit volume of the CL (see Eq. A.22). The volumetric production of protonic current density $\nabla\cdot i$ can be replaced by di/dz for the present 1D analysis. For this purpose the volumetric source term is corrected as

$$\frac{di}{dz} = -4FR_{O_2}\frac{A}{a} \tag{18}$$

therefore

$$\frac{di}{dz} = 4F\left(\frac{1}{Ek_1A} + \frac{\delta_{agg}}{a_{agg}D_{O_2,m}}\frac{r_{agg}+\delta_{agg}}{r_{agg}}\right)^{-1}\frac{c_{O_2}}{K_{O_2}} \tag{19}$$

The first order reaction rate constant k_1 is related to an activation overpotential η and exchange current density i_0 via Butler–Volmer equation [21]

$$k_1 = \frac{1}{4F}\frac{i_{0,\text{ref}}}{c_{O_2}^{\text{ref}}}\left[\exp\left(\frac{\alpha_cF}{RT}\eta\right) - \exp\left(-\frac{\alpha_aF}{RT}\eta\right)\right] \tag{20}$$

$i_{0,\text{ref}}$ is calculated from a relationship provided in Ref. [23] and is equal to $1.76\times10^{-4}\,\text{A m}^{-2}$.

2.2. Oxygen diffusion

The oxygen diffusion is modeled using oxygen molar conservation and Fick's law of diffusion,

$$\frac{dc_{O_2}}{dz} = \frac{i - I_\delta}{4FD_{O_2}^{\text{eff}}} \tag{21}$$

where I_δ and $D_{O_2}^{eff}$ are the cell current density and the overall effective oxygen gas diffusion coefficient within the CL, respectively. Liquid water exists in the cathode CL as a result of a oxygen reduction reaction (ORR). It may be partially or fully flooded in the secondary pores. Therefore, the gas pores shrink and the resistance against oxygen gas diffusion increases. Oxygen gas can reach the agglomerate surface by two processes: (1) through the liquid water flooded in the pores (denoted by s) and (2) through open fraction of pores (denoted by $(1-s)$). To take into account the effect of liquid water in the pores, a parallel model for calculating the oxygen diffusion coefficient is considered as

$$D_{O_2}^{\text{eff}} = D_{O_2-g}^{\text{eff}}\frac{(1-s)\varepsilon_c}{\varepsilon_c + L_{g,c}(1-\varepsilon_g)} + D_{O_2-w}^{\text{eff}}\frac{s\varepsilon_c}{\varepsilon_c + L_{g,c}(1-\varepsilon_g)} \tag{22}$$

where $D_{O_2-g}^{eff}$ is the effective oxygen gas diffusion coefficient showing diffusion through gas pores (see Appendix A). $D_{O_2-w}^{eff}$ is related to its bulk value, i.e., dissolved oxygen diffusion coefficient in liquid water D_{O_2-w}, as [22]

$$D_{O_2-w}^{\text{eff}} = (\varepsilon_c s)^\tau D_{O_2-w} \tag{23}$$

2.3. Activation overpotential

There exists a resistance to protons and electrons migrating through the polymer and solid portions of a CL. The activation overpotential can be described by Ohm's law

$$\frac{d\eta}{dz} = \frac{i}{\kappa^{\text{eff}}} + \frac{i - I_\delta}{\sigma^{\text{eff}}} \tag{24}$$

where κ^{eff} and σ^{eff} are the effective protonic and electrical conductivities. The effective conductivities are obtained by employing the Bruggeman correlation [24]

$$\kappa^{\text{eff}} = (1-\varepsilon_c)\left(1 + \frac{\varepsilon_{agg}-1}{(1+\delta_{agg}/r_{agg})^3}\right)\kappa \tag{25}$$

$$\sigma^{\text{eff}} = (1-\varepsilon_c - L_{m,c})^\tau\sigma \tag{26}$$

Eqs. (19), (21) and (24) comprise a coupled system of nonlinear ODE's with the unknowns i, C_{O_2} and η that govern the transport of oxygen, protons and electrons within an agglomerate CL. To solve the ODE's, we need to specify several boundary conditions for the unknowns (see below).

2.4. Boundary conditions

All of the Boundaries are shown in Fig. 1. The oxygen concentration at the GDL/CL interface is determined using the ideal gas law

$$C_{O_2}\,|\,z=0 = \frac{P_{O_2}}{\bar{R}T} \tag{27}$$

in which P_{O_2} is the oxygen partial pressure at the GDL/CL interface. Oxygen is consumed in the CL as a result of ORR, and its mole fraction decreases along the GDL thickness from the gas channel to the CL. Reduction in the oxygen mole fraction and therefore in P_{O_2} is obtained by modeling of the gas species transport in the GDL. Mathematical modeling of all mass transport processes occurring in the GDL is performed using the Maxwell–Stefan equations for the diffusion of multi-component ideal gasses [31,32]

$$\nabla x_i = \sum_{j=1}^{n}\frac{\bar{R}T}{PD_{ij}^{\text{eff}}}\left(x_iN_{j,g} - x_jN_{i,g}\right)\quad i = 1,\ldots,n-1 \tag{28}$$

x is the species mole fraction, $\bar{R}$ is the universal gas constant ($=8.3143\,J\,mol^{-1}\,K^{-1}$), T is the temperature which is constant in this isothermal computation, P is the gas mixture pressure, and N is the species molar flux defined using superficial velocity components. The subscript i takes a value of 1, 2 or 3 and is related to O_2, H_2O_g, and N_2, respectively. D_{ij}^{eff} is the effective binary diffusion coefficient within the GDL and is related to the binary diffusion D_{ij} by [22]

$$D_{ij}^{\text{eff}} = D_{ij}\varepsilon_g^{3/2} \tag{29}$$

Two other boundary conditions are defined for the protonic current densities at the GDL/CL and CL/membrane interfaces:

$$i|_{z=0} = 0 \qquad i|_{z=l_c} = I_\delta \tag{30}$$

To fully consider the effects of the CL agglomerate structure, a number of parameters must be defined (see derivation in Appendix A).

3. Optimization methodology using harmony search algorithm

The harmony search (HS) algorithm [25,26], which is a newly developed optimization method, is utilized to determine the minimum activation overpotential, η. This algorithm is conceptually simple, involves only a few parameters, and can be easily implemented. It has been successfully applied to various benchmark and real-world optimization problems [27–29]. In the following subsections the optimization methodology is described in brief. More details about the algorithm can be found in Refs. [25,29]. An interested reader can download the source code of the HS algorithm written in MATLAB from the authors' web page [30].

3.1. Objective function

The objective of the optimization problem is to minimize the CL activation overpotential, η. To calculate η, one needs to solve the coupled system of ordinary differential equations (ODEs), that is, Eqs. (19), (21) and (24).

3.2. Design variables

Design variables and the associated ranges are given in Table 1.

3.3. Solution methodology

Firstly, the initial values of the design variables are randomly assigned by the HS within the defined respective ranges. A simulation is then done to calculate the η of a specified PEMFC. The HS algorithm, based on the obtained results from the first simulation, sets new values of the design variables and another simulation is performed to evaluate the η of the new design. The new values of the design variables can be chosen either randomly or by using the best obtained values, which are already stored in the algorithm's harmony memory. If η of the new design is less than the worst solution available in the harmony memory, the new solution replaces the worst solution in the harmony memory. As the optimization process proceeds, little by little, the solutions stored in harmony memory approach an optimum solution. The process is continued until a pre-specified maximum number of iterations for the HS algorithm is reached. More details about the harmony search can be found in Refs. [25,26].

Table 1
Input parameters and their corresponding values used in this work.

Input parameters	Level 1	Level 2	Level 3
s	0	0.6	1
δ_{agg}	0	40×10^{-9}	80×10^{-9}
r_{agg}	5×10^{-9}	5×10^{-7}	1×10^{-6}
m_{Pt}	0.04	0.05	0.06
m_c	0.002	0.003	0.004
$L_{m,c}$	0.05	0.3	0.4
$L_{g,c}$	0.05	0.1	0.15
ε_g	0.3	0.4	0.45
l_c	1×10^{-5}	3.5×10^{-5}	7×10^{-5}

4. Results and discussion

4.1. Main effects of the input parameters

The main effects plot of each input parameter (shown in Table 1) on the CL activation overpotential is shown in Fig. 2. The ANOM value for each level of a parameter is an average determined while all other parameter levels are varied. The ANOM plot shows the average trend of the CL activation overpotential versus each input parameter. A reference line, shown in Fig. 2, is a horizontal line, which is drawn at the grand mean (the average CL activation overpotential for all input parameters). In Fig. 2 a general trend of the mean activation overpotential versus each input parameter is displayed.

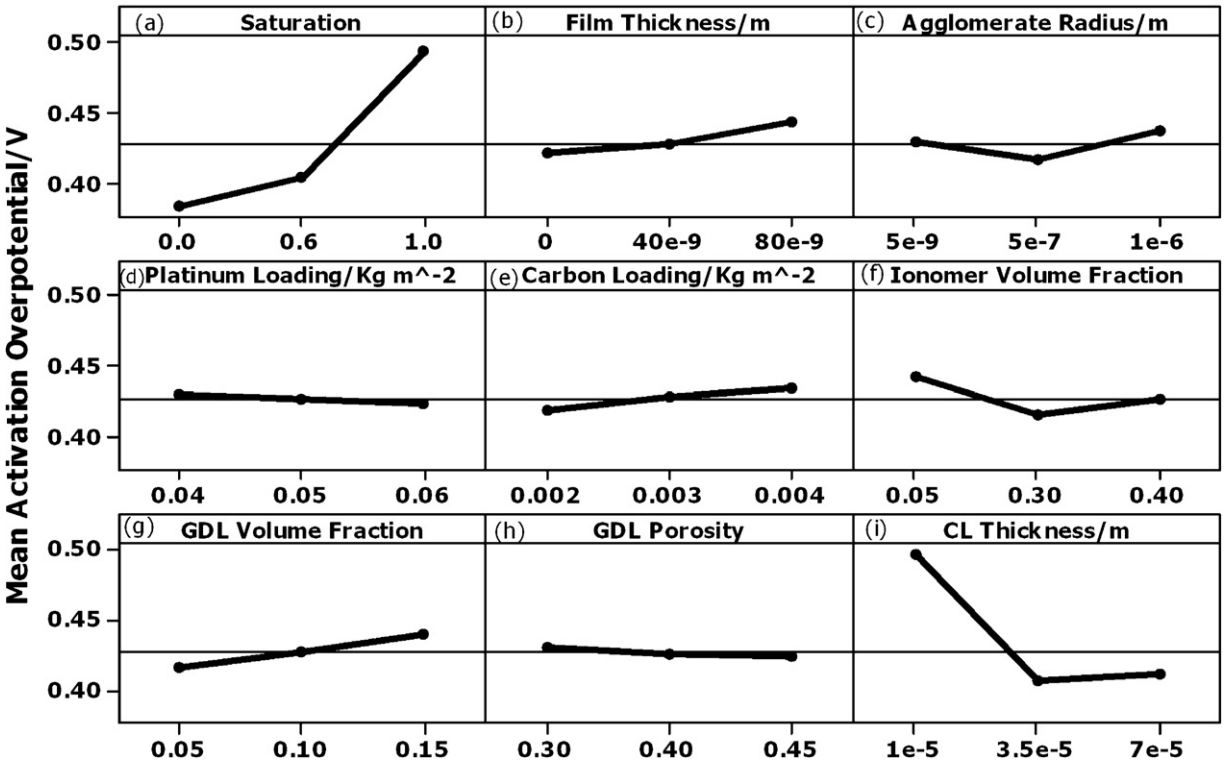

Fig. 2. Main effects of the input parameters (ANOM plot).

The mean activation overpotential increases as the liquid water saturation increases (see Fig. 2(a)). Increasing liquid water saturation reduces the effective oxygen diffusion coefficient by limiting the oxygen diffusion and accessible area to pass through. If this plot is compared to other subplots, it can be seen that saturation has the greatest effect on the activation overpotential. The CL performance is reduced by 30% when the liquid water saturation is increased from $s = 0$ to $s = 1$, which corresponds to the situations of open and fully flooded pores, accordingly.

The average effects of the agglomerate ionomer film thickness on the CL activation overpotential are shown in Fig. 2(b). Although an ionomer film is necessary on the surface of an agglomerate to provide pathways for protons to reach the reaction sites on the surface, Fig. 2(b) shows that the increasing ionomer film thickness increases the mean CL activation overpotential due to the increased diffusion length.

The main effect of the agglomerate radius on the mean CL activation overpotential is displayed in Fig. 2(c). The mean CL activation overpotential initially decreases and then increases as the agglomerate radius increases. In other words, there is an optimum value for the agglomerate radius, which maximizes the CL performance. The agglomerate radius affects a number of parameters, namely, the number of agglomerates n_{agg}, tortuosity τ, the ionomer volume fraction inside the agglomerates ε_{agg}, the external active surface area a_{agg}, the active surface area within the agglomerates a, and the diameter of the pores between the agglomerates d_{avg}. As the agglomerate radius increases the diffusion length of dissolved oxygen inside the agglomerate increases as well (see Eq. (19)) but tortuosity decreases (see Eq. A.26). The former effect tends to deteriorate the CL performance whilst the latter tends to enhance the CL performance. The net effect is as shown in Fig. 2(c).

Fig. 2(d) and (e) demonstrate that the main effects of the platinum mass loading m_{Pt} and carbon mass loading m_C on the CL activation overpotential are almost linear. The linear main effects indicate that only two levels, i.e., the minimum and the maximum values, of these two input parameters are enough to find their corresponding main effect variations. Furthermore, Fig. 2(d) shows that an increase in the platinum mass loading reduces the activation overpotential. This effect is due to the increased active reaction area. On the other hand, Fig. 2(e) shows that an increase in the carbon mass loading increases the activation overpotential due to limiting of the CL porosity.

The average changes of activation overpotential in response to changes in the ionomer volume fraction of the CL are displayed in Fig. 2(f). As the CL ionomer volume fraction increases, the mean CL activation overpotential decreases at first, and then increases. This behavior implies that there is an optimum for the CL ionomer volume fraction. This can be explained by the fact that as the ionomer volume fraction increases inside the CL, the porosity reduces and the agglomerate ionomer volume fraction increases. The two effects compete and the net result is shown in Fig. 2(f).

The main effects of the GDL penetration content in the CL and its porosity are shown in Fig. 2(g) and (h), respectively. The mean activation overpotential increases with respect to GDL penetration content and decreases with an increase in GDL porosity. In other words, the added GDL volume fraction in the CL (as a result of compression in membrane electrode assembly (MEA) process) deteriorates the CL performance. This is due to the penetration of solid material of GDL into the CL and therefore to a limitation of CL porosity. However, a higher GDL porosity increases the CL porosity (through the last term in Eq. (A.12)) and enhances the CL performance.

Fig. 2(i) shows the main effects of the CL thickness on the mean activation overpotential. The CL thickness is changed from 10 to 70 μm [37]. It can be seen that the activation overpotential initially decreases and reaches minimum, and then slightly increases as the CL becomes thicker. Increasing the CL thickness has two main competing effects. Firstly, it increases the CL porosity which decreases the activation overpotential. Secondly, it increases the diffusion length of oxygen and consequently it gives rise to the diffusion resistance resulting in an increase of the activation overpotential.

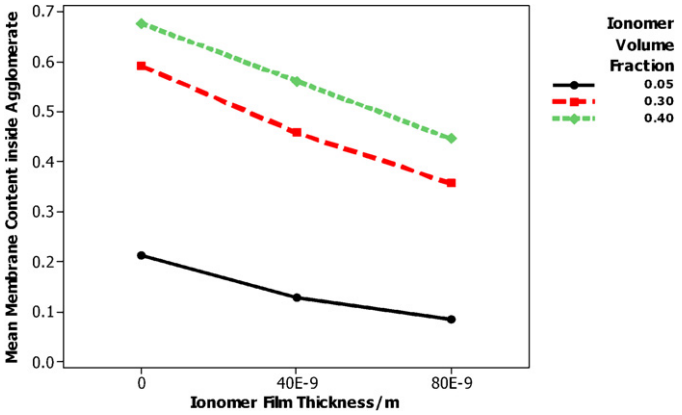

Fig. 3. Interaction plot of ionomer film thickness and ionomer volume fraction on mean ionomer volume fraction inside agglomerate.

4.2. Interaction plots

An interaction plot is a plot of means for each level of an input parameter with a level of a second input parameter being constant. An interaction exists when lines in an interaction plot are not parallel. Parallel lines indicate no interaction, i.e., response to an input factor does not depend upon the level(s) of the other input parameters. The greater the divergence of the lines from parallel is, the higher is the degree of interaction obtained [38]. Presence of interactions indicates important implications for the interpretation of data, i.e., one thing that cannot be brought up by main effects plots. Generally, if two input parameters interact, the relationship between each interacting input parameter and the third dependent variable, i.e., activation overpotential, depends on the value of the other interacting input parameter. This makes it difficult to predict consequences resulting as an input parameter's value changes, especially if the variable it interacts with is hard to measure.

Fig. 3 displays the ionomer thickness δ_{agg} and ionomer volume fraction $L_{m,c}$ interaction on the mean ionomer volume fraction inside agglomerate ε_{agg}. The profiles are almost parallel and therefore do not indicate any significant interaction. In other words, the effect of ionomer film thickness on the agglomerate ionomer volume fraction is not dependent on the CL ionomer volume fraction. Having looked at the main effects plot, one would not recognize any possible interactions. In addition, it can be seen that the mean ionomer volume fraction inside the agglomerates ε_{agg} reduces as the ionomer film thickness δ_{agg} increases at each CL ionomer volume fraction level $L_{m,c}$. It results in the effective protonic conductivity reduction inside each agglomerate κ^{eff} (see Eq. (25)).

Interaction between the GDL porosity and GDL volume fraction ($\varepsilon_g \times L_{g,c}$) for activation overpotential is plotted in Fig. 4, in which the non parallel lines indicate an interaction. Fig. 4 shows that the effects of GDL porosity on activation overpotential depend on the GDL penetration content.

To explain more the influence of CL thickness, the interactions plots of CL thickness with platinum loading and ionomer volume fraction are shown separately in Figs. 5 and 6.

The interaction plot of CL thickness and platinum loading on the CL activation overpotential in Fig. 5 shows that a higher platinum mass loading does not necessarily lower the CL activation overpotential. This is due to the trade-off between porosity and the

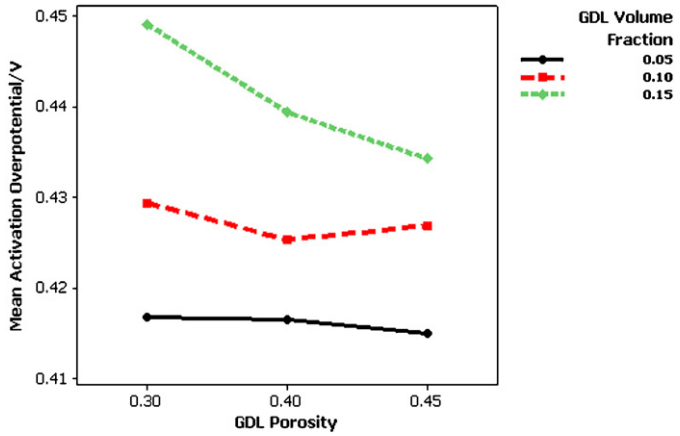

Fig. 4. Interaction plot of GDL porosity and GDL penetration volume fraction on mean activation overpotential.

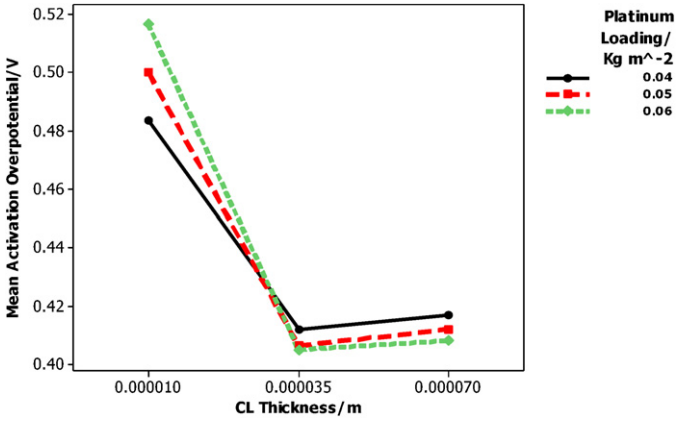

Fig. 5. Interaction plot of CL thickness and platinum loading on mean activation overpotential.

reaction surface area. There is a mid-range value for the CL thickness, in which the highest platinum loading results in the lowest loss. The interaction plot of the CL thickness and the ionomer volume fraction on CL activation overpotential in Fig. 6 demonstrates strong interaction of these two input parameters. The lowest activation overpotential is obtained when the CL thickness and the ionomer volume fraction values are in the mid-range of their corresponding intervals.

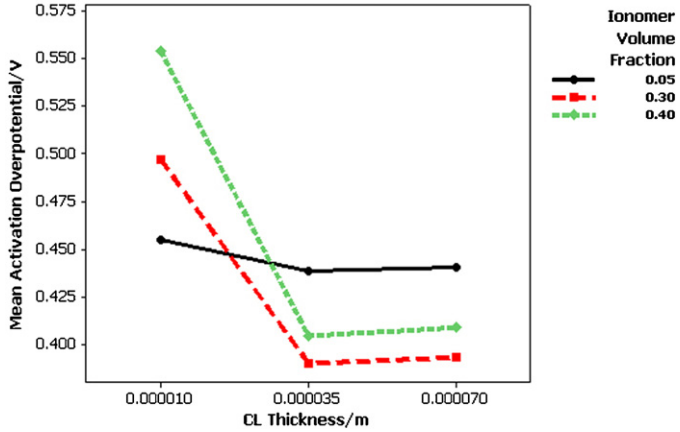

Fig. 6. Interaction plot of CL thickness and ionomer volume fraction on mean activation overpotential.

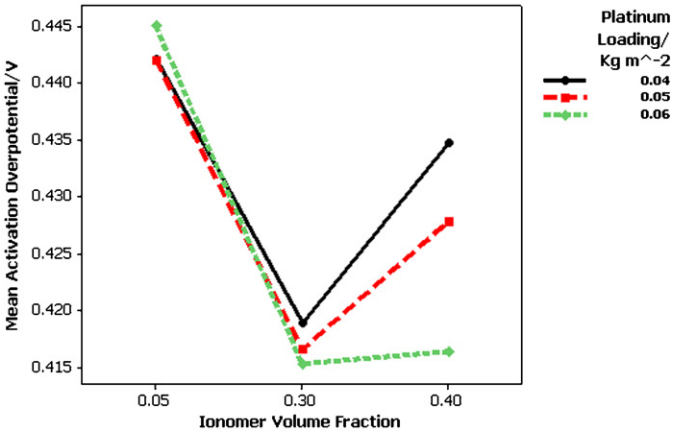

Fig. 7. Interaction plot of ionomer volume fraction and platinum loading on mean activation overpotential.

The interaction plot of ionomer volume fraction $L_{m,c}$ and platinum loading m_{Pt} on the mean activation overpotential is shown in Fig. 7. The highly non-parallel profiles indicate significant interactions between $L_{m,c}$ and m_{Pt}. In other words, the effects of ionomer volume fraction on the activation overpotential depend on the amount of platinum loading, especially for high ionomer volume fraction values. This is also discussed by Sasikumar et al. [13], and by Yin [14]. To better illustrate this, a contour plot of the mean activation overpotential versus the ionomer volume fraction and platinum loading is shown in Fig. 8. Each patterned zone corresponds to a range of the activation overpotential and the black dots shows the main levels of $L_{m,c}$ and m_{Pt}, shown in Table 1. Generally, the lower the activation overpotential is, the better the CL performance is at high ionomer volume fraction and platinum loadings. However, an optimum design may not be obtained at the highest ionomer volume fraction and platinum loading values. The reason is that the optimum ionomer volume fraction and platinum loading depends on the values of other parameters as a result of possible interaction with them.

4.3. ANOVA table

To determine the significance of each input parameter on the CL performance, an analysis of variance (ANOVA) is performed. The data obtained in this study are summarized in Table 2. The components of the ANOVA table are explained as follows[33].

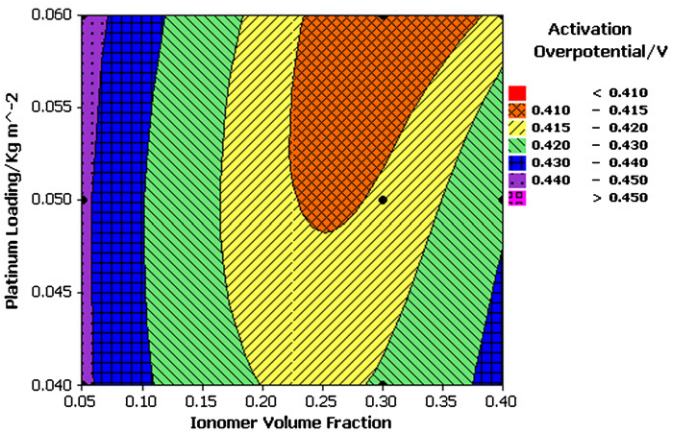

Fig. 8. Contour plot of activation overpotential versus platinum loading and ionomer volume fraction.

Table 2
The analysis of variance (ANOVA).

Source	DF	SS	MS	*F*
s	2	26.5986	13.2993	2306.79
δ_{agg}	2	5.7153	2.8576	495.66
r_{agg}	2	0.8840	0.4420	76.66
m_{Pt}	2	0.0002	0.0001	0.02
m_c	2	1.2701	0.6350	110.15
$L_{m,c}$	2	3.3410	1.6705	289.75
$L_{g,c}$	2	1.8727	0.9363	162.41
ε_g	2	0.1313	0.0657	11.39
l_c	2	17.5262	8.7631	1519.97
Error	11,379	65.6032	0.0058	
Total	11,379	116.2923		

- *Source*: indicates each input parameter
- *DF*: degree of freedom, which is the number of each level minus one
- *SS*: sum of squares between the input parameters
- *MS*: mean squares obtained by (SS/DF)
- *F*: calculated dividing the MS of each input parameter by the error MS

The *F*-value illustrates how significant a given input parameter is. A *F*-value higher than 4 means that the effect is "strong"; if it is less than 1 it means that the effect is negligible [38]. A value in between, i.e., $1 < F < 4$ means that the effect is mild. As seen on Table 2, saturation and CL thickness have the highest influence on the CL performance. The ionomer film thickness, CL ionomer volume fraction, GDL volume fraction inside the CL, carbon loading, agglomerate radius, and GDL porosity also have significant effects on the CL performance. The effects of platinum loading on the CL performance for the given short range of platinum loading are small. In this study the range of change of the platinum mass loading is small since there is a cost limitation of platinum usage for manufacturers.

4.4. Optimization results

The HS algorithm is applied to find the optimum values of the input parameters in their base case ranges (see Table 1) which result in optimum performance (minimum CL activation overpotential, η). Table 3 shows the optimum solution. It can be seen that the optimum performance is achieved at several intermediate points for the agglomerate radius r_{agg}, ionomer volume fraction $L_{m,c}$, and one of the endpoints of other parameter ranges.

The optimum solution is obtained when the platinum loading is at a maximum. In cases where the m_{Pt} is less than maximum, η increases. We can add another objective function, such as minimum platinum loading, to the problem to find if a trade-off between two objectives exists. A solution of the multi objective optimization problem is called Pareto optimal if there exist no feasible vectors of design variables, which would lower one

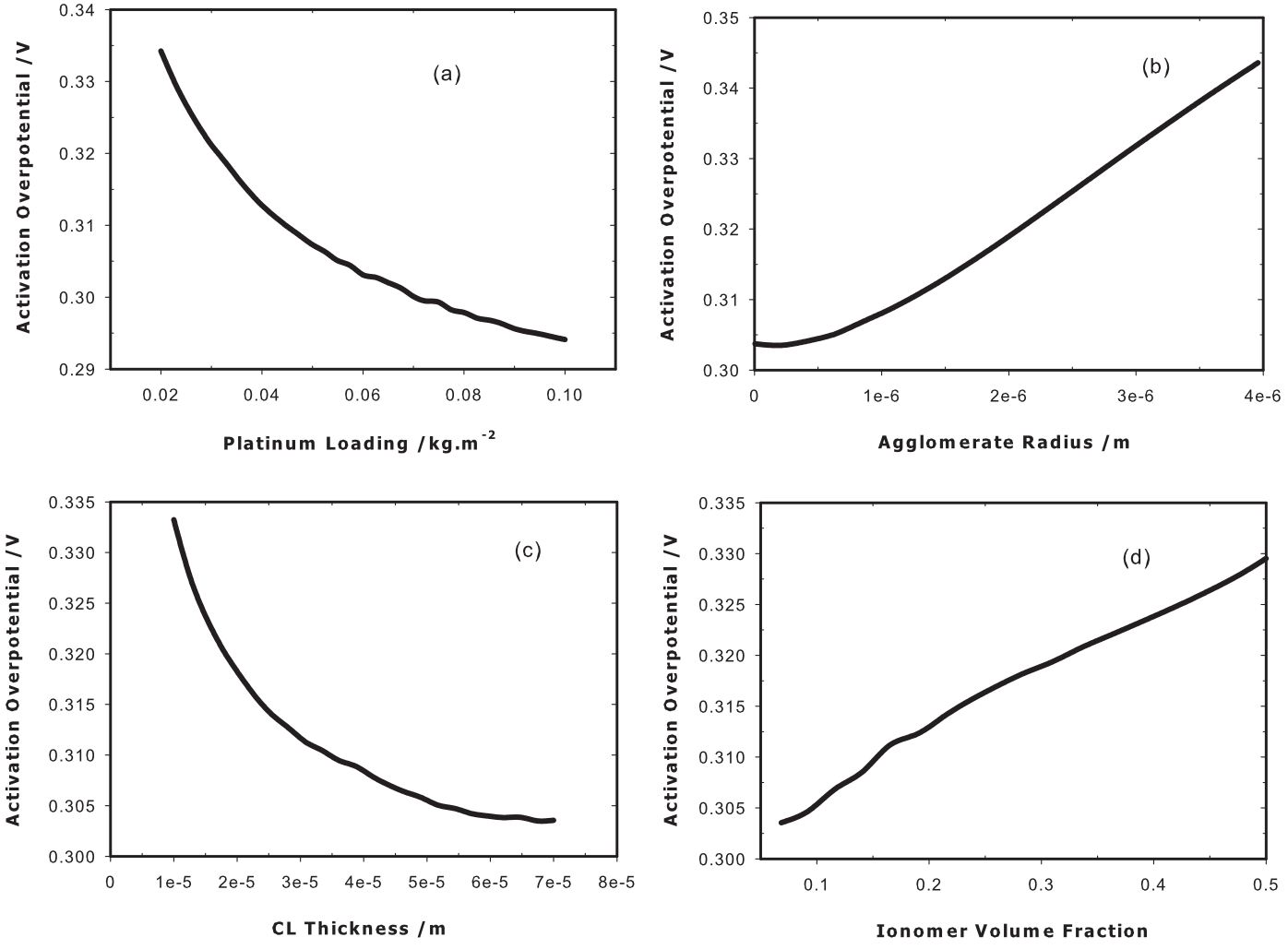

Fig. 9. Pareto plot.

Table 3
Optimum input parameters' values and corresponding activation overpotential.

Variables	s	δ_{agg}	r_{agg}	m_{Pt}	m_c	$L_{m,c}$	$L_{g,c}$	ε_g	l_c	η
Optimum values	0	0	3.47×10^{-8}	0.06	0.002	0.074	0.05	0.45	7×10^{-5}	0.303

objective without causing a simultaneous increase in at least one other objective. Pareto optimal sets are called non-dominated. The plot of the objective functions whose non-dominated vectors are in the Pareto optimal set is called the Pareto front [36]. Fig. 9 shows the Pareto front for the η and m_{Pt}, r_{agg}, l_c, and $L_{m,c}$. As it can be seen in Fig. 9, the optimum CL activation overpotential decreases with an increase in m_{Pt}. The final optimum solution among the optimum points existing on the Pareto front needs to be selected by a decision-making process. In fact, the selection process is usually based on engineering experience and importance of each objective for decision makers. The Pareto optimal front for η versus r_{agg} is shown in Fig. 9(b). It shows that any increase in r_{agg} results in an increase in the optimum η. While an increase in l_c leads to a better optimum value (Fig. 9(c)), an increase in $L_{m,c}$ monotonically increases the optimum value for η (Fig. 9(d)).

5. Conclusions

A comprehensive mathematical model for the homogenous agglomerate CL was developed to investigate the effects of nine CL parameters on the CL activation overpotential. These parameters include saturation (s) and eight structural parameters (δ_{agg}, r_{agg}, m_{Pt}, m_C, $L_{m,c}$, $L_{g,c}$, ε_g and l_c). An analysis of means was performed to show the main effect of the CL activation overpotential with respect to each parameter. The potential interaction between parameters was analyzed using interaction plots. They show strong interaction between m_{Pt}, $L_{m,c}$, and l_c on activation overpotential. Using the ANOVA method, saturation and CL thickness were found to be the most influential parameters affecting the CL performance. In addition, the HS algorithm was used to find the optimum values of input parameters. It was found that the optimum performance was achieved at several intermediate points for the agglomerate radius and the ionomer volume fraction and at one of the endpoints of other parameter ranges.

Acknowledgements

This work had been partly supported by the ENERGY-GCOE program at Tokyo Institute of Technology and the Grant-in-Aid for Scientific Research from MEXT/JSPS. The authors also thank L. Afanasieva and Paul Iliffe for their comments and suggestions.

Appendix A.

First, a relationship between the volume of the existing material and open pores in the CL needs to be defined. Having noted that each agglomerate has a nucleus (with a diameter of r_{agg}) and an ionomer film covering the nucleus (with thickness of δ_{agg}), the following relationships between the volumes can be established

$$V_{tot} = V_m + V_C + V_{Pt} + V_p + V_s \tag{A.1}$$

$$V_{agg} = V_C + V_{Pt} + V_m|_{nucleus} \tag{A.2}$$

$$V_m = V_m|_{nucleus} + n'_{agg}\frac{4}{3}\pi\left[\left((r_{agg}+\delta)^3 - r_{agg}^3\right)\right] \tag{A.3}$$

where n'_{agg} is the number of agglomerate within the CL. The following parameters are also employed in the mathematical model

$$\varepsilon_c = \frac{V_p}{V_{tot}} \tag{A.4}$$

$$L_m = \frac{V_m}{V_{tot}} \tag{A.5}$$

$$\varepsilon_{agg} = \frac{V_m|_{nucleus}}{V_{agg}} \tag{A.6}$$

$$L_s = \frac{V_s}{V_{tot}} \tag{A.7}$$

A.1. CL porosity

A relationship for the CL porosity can be developed using Eq. (A.2) with respect to catalyst particle masses

$$V_{agg} = \frac{(mass)_{Pt}}{\rho_{Pt}} + \frac{(mass)_C}{\rho_C} + V_m + V_s \tag{A.8}$$

Dividing both sides of the above relationship by the total CL volume which is $V_{tot} = A_c l_c$ gives

$$\frac{V_{agg}}{V_{tot}} = \frac{(mass)_{Pt}}{\rho_{Pt}A_c l_c} + \frac{(mass)_C}{\rho_C A_c l_c} + L_m + L_{g,c}(1-\varepsilon_g) \tag{A.9}$$

Having noted that the left hand side is equal to $(1-\varepsilon_c)$, and $(mass)/A_c$ denotes loading, rearranging gives

$$\varepsilon_c = 1 - \frac{1}{l_c}\left(\frac{m_{Pt}}{\rho_{Pt}} + \frac{m_C}{\rho_C}\right) - L_m - L_{g,c}(1-\varepsilon_g) \tag{A.10}$$

Introducing f as a mass fraction of the platinum to that of the Pt/C particles

$$f \equiv \frac{m_{Pt}}{m_{Pt}+m_C}, \tag{A.11}$$

gives a relationship for m_C in terms of m_{Pt}. Then, the CL porosity can be rewritten as

$$\varepsilon_c = 1 - \frac{m_{Pt}}{l_c}\left(\frac{1}{\rho_{Pt}} + \frac{1-f}{1}\frac{1}{\rho_C}\right) - L_m - L_{g,c}(1-\varepsilon_g) \tag{A.12}$$

A.2. Calculation of n_{agg}

n_{agg} is the number of agglomerates per total volume of the CL. In order to derive a relationship for n_{agg}, Eqs. (A.2) and (A.3) are substituted into Eq. (A.1), and then is divided by V_{tot}. Rearranging gives

$$1 = n_{agg}\left[\frac{4}{3}\pi r_{agg}^3 + \frac{4}{3}\pi\left((r_{agg}+\delta_{agg})^3 - r_{agg}^3\right)\right] + \varepsilon_c \tag{A.13}$$

In the derivation of the above equation, V_{agg} for the spherical geometry is replaced by

$$V_{agg} = n'_{agg}\left(\frac{4}{3}\right)\pi r_{agg}^3 \tag{A.14}$$

Solving Eq. (A.13) for n_{agg} gives:

$$n_{agg} = \frac{n'_{agg}}{V_{tot}} = \left[\frac{4}{3}\pi\left(r_{agg}+\delta_{agg}\right)3\right] - 1(1-\varepsilon_c) \tag{A.15}$$

A.3. Ionomer volume fraction inside the agglomerate

A relationship for the ionomer volume fraction inside agglomerates is obtained by dividing both sides of Eq. (A.3) by the total CL volume and gives

$$\frac{V_m}{V_{tot}} = \frac{V_m|_{nucleus}}{V_{tot}} + \frac{n'_{agg}}{V_{tot}}\frac{4}{3}\pi\left[\left((r_{agg}+\delta_{agg})^3 - r_{agg}^3\right)\right] \tag{A.16}$$

The first term on the right side can be written as

$$\frac{V_m|_{\text{nucleus}}}{V_{\text{tot}}} = \frac{V_m|_{\text{nucleus}}}{V_{\text{agg}}}\frac{V_{\text{agg}}}{V_{\text{tot}}} = \varepsilon_{\text{agg}}\frac{V_{\text{agg}}}{V_{\text{tot}}} \tag{A.17}$$

Substituting Eq. (A.17) in Eq. (A.16) and solving for ε_{agg} gives

$$\varepsilon_{\text{agg}} = \frac{L_{m,c} + n_{\text{agg}}(4/3)\pi r_{\text{agg}}^3}{n_{\text{agg}}(4/3)\pi(r_{\text{agg}} + \delta_{\text{agg}})^3} - 1 \tag{A.18}$$

A.4. Calculation of A and A_s and a_{agg}

A_s is the reaction surface area per unit mass of platinum and is a function of f [23]

$$A_s = (227.79f^3 - 158.57f^2 - 201.53f + 159.5) \times 10^3 \tag{A.19}$$

The total active area of agglomerates per unite volume of the CL A can be obtained as [34]

$$A = \frac{m_{\text{Pt}}}{l_c}A_s \tag{A.20}$$

a_{agg} defined as the external area of active sites of agglomerates per volume of the CL is given by

$$a_{\text{agg}} = 4\pi r_{\text{agg}}^2 n_{\text{agg}} \tag{A.21}$$

Finally, the active surface area within the agglomerates can be calculated using Eqs. (A.14) and (A.15) as

$$a = A\frac{V_{\text{tot}}}{V_{\text{agg}}} = \frac{A}{n_{\text{agg}}(4/3)\pi r_{\text{agg}}^3} \tag{A.22}$$

A.5. Knudsen diffusion

In the CL, when the agglomerates radii are small, pore diameters may be very small, comparable to mean free path of oxygen molecule. Therefore, a Knudsen diffusion prevails. The Knudsen number is defined as

$$Kn = \frac{\lambda}{d_{\text{avg}}} \tag{A.23}$$

where λ denotes the mean free path and is a function of temperature and pressure

$$\lambda = \frac{k_B T}{\sqrt{2}\pi\sigma_{ii}P} \tag{A.24}$$

where k_B and σ_{ii} are the Boltzmann constant and collision diameter. The mean free path for oxygen molecule at T = 353 K and P = 5 atm is 2.4×10^{-8} m. The average pore diameter in the CL, d_{avg}, is obtained as [35]

$$d_{\text{avg}} = \frac{4}{3}\frac{\varepsilon_c}{1-\varepsilon_c}r_{\text{agg}} \tag{A.25}$$

Tortuosity is a function of the average pore diameter and is calculated by [39,16]

$$\tau = \frac{1}{\varepsilon_c} + 1.196\frac{\sigma_{dev}}{d_{\text{avg}}} \tag{A.26}$$

In this study, the Knudsen effect is taken into account when the Knudsen number Kn is greater than 0.1. The Knudsen diffusion is determined from the kinetics theory and is calculated by

$$D_{\text{Kn}} = \frac{1}{3}d_{\text{avg}}\sqrt{\frac{8RT}{\pi M_{O_2}}} \tag{A.27}$$

Then, the equivalent diffusion coefficient of oxygen gas in the micro and nano pores of the CL is obtained from

$$\frac{1}{D_{O_2-g,e}} = \frac{1}{D_{O_2-g}} + \frac{1}{D_{\text{Kn}}} \tag{A.28}$$

where D_{O_2-g} is the bulk oxygen gas diffusion coefficient in its mixture with nitrogen and water vapor gases and is calculated by

$$D_{O_2-g} = \frac{1 - x_{O_2}}{\frac{x_{N_2}}{D_{O_2-N_2}} + \frac{x_{H_2O}}{D_{O_2-H_2O}}} \tag{A.29}$$

In order to take the effect of porosity and tortuosity into account, the Brugmann correction factor is employed

$$D_{O_2-g}^{\text{eff}} = D_{O_2-g,e}(\varepsilon_c(1-s))^{\tau} \tag{A.30}$$

The bulk diffusion coefficients are given in Refs. [23,40].

References

[1] D.M. Bernardi, M.W. Verbrugge, J. Electrochem. Soc. 139 (1992) 1477.
[2] J. Larminie, A. Dicks, Fuel Cell Systems Explained, John Wiley & Sons, Toronto, 2000.
[3] P.K. Das, X. Li, Z.S. Liu, J. Power Sources 179 (2008) 186.
[4] D. Song, Q. Wang, Z. Liu, M. Eikerling, Z. Xie, T. Navessin, S. Holdcroft, Electrochim. Acta 50 (2005) 3347.
[5] H. Bahrami, A. Faghri, Int. J. Heat Mass Transfer 53 (2010) 2563.
[6] H. Bahrami, A. Faghri, J. Fuel Cell Sci. Technol. 8 (2011) 015006.
[7] N.P. Siegel, M.W. Ellis, D.J. Nelson, M.R. von Spakovsky, J. Power Sources 115 (2003) 81.
[8] F. Liu, B. Yi, D. Xing, J. Yu, Z. Hou, F. Fu, J. Power Sources 124 (2003) 81.
[9] S.J. Lee, S. Mukerjee, J. McBreem, Y.W. Rho, Y.T. Kho, T.H. Lee, Electrochim. Acta 43 (1998) 3693.
[10] S.J. Ridge, R.E. White, Y. Tsou, R.N. Beaver, G.A. Eisman, J. Electrochem. Soc. 136 (1989) 1902.
[11] Q. Wang, M. Eikerling, D. Song, Z. Liu, J. Electroanal. Chem. 573 (2004) 61.
[12] W. Sun, B.A. Peppley, K. Karan, Electrochim. Acta (50) (2005) 3359.
[13] G. Sasikumar, J.W. Ihm, H. Ryu, J. Power Sources 132 (2004) 11.
[14] K.M. Yin, J. Electrochem. Soc. 152 (2005) A583.
[15] M. Secanell, K. Karan, A. Suleman, N. Djilali, Electrochim. Acta 52 (2007) 6318.
[16] S. Kamarajugadda, S. Mazumder, J. Power Sources 183 (2008) 629.
[17] R. Madhusudana Rao, D. Bhattacharyya, R. Rengaswamy, S.R. Choudhury, J. Power Sources 173 (2007) 375.
[18] O. Levenspiel, Chemical Reaction Engineering, 3rd ed., John Wiley & Sons, New Jersey, 1999.
[19] D. Songa, Q. Wang, Z. Liu, T. Navessin, M. Eikerling, S. Holdcroft, J. Power Sources 126 (2004) 104.
[21] F. Barbir, PEM Fuel Cells: Theory and Practice, University of California, Davis/Elsevier Academic Press, 2005.
[22] R.E. De la Rue, C.W. Tobias, J. Electrochem. Soc. 106 (1959) 827.
[23] N. Khajeh-Hosseini-Dalasm, M.J. Kermani, D. Ghadiri Moghaddam, J.M. Stockie, Int. J. Hydrogen Energy 35 (2010) 2417.
[24] F. Jaouen, G. Lindbergh, G. Sundholm, J. Electrochem. Soc 149 (4) (2002) A437.
[25] K.S. Lee, Z.W. Geem, Comput. Method Appl. M 194 (2004) 3902.
[26] M. Mahdavi, M. Fesanghary, E. Damangir, Appl. Math. Comput. 188 (2007) 1567.
[27] A. Vasebi, M. Fesanghary, S.M.T. Bathaee, Int. J. Electr. Power 29 (2007) 713.
[28] H. Ceylan, H. Ceylan, S. Haldenbilen, O. Baskan, Energy Policy 36 (2008) 2527.
[29] M. Fesanghary, M. Mahdavi, M. Minary, Y. Alizadeh, Comput. Method Appl. M 197 (2008) 3080.
[30] M. Fesanghary, 2011, January 18, 2011, https://sites.google.com/site/fesangharyweb/downloads.
[31] R.B. Bird, W.E. Stewart, E.N. Lightfoot, Transport Phenomena, Wiley, New York, 2002.
[32] H. Bahrami, A. Faghri, J. Electrochem. Soc 157 (12) (2010) B1762.

[33] S. Ahadian, H. Mizuseki, Y. Kawazoe, Microfluid. Nanofluid. 9 (2010) 319.
[34] J.J. Baschuk, X. Li, J. Power Sources 86 (2000) 181.
[35] D.G. Huizenga, D.M. Smith, AIChE J. 32 (1986) 1.
[36] K. Deb, A. Pratap, S. Agarwal, T. Meyarivan, Technical Report 2000001, Kanpur Genetic Algorithms Laboratory (KanGAL), Indian Institute of Technology Kanpur, 2000.
[37] Q. Wang, D. Song, T. Navessin, S. Holdcroft, Z. Liu, Electrochim. Acta 50 (2004) 725.
[38] Minitab, Minitab Reference Manuel, Minitab, Inc, USA, 2010.
[39] M.H. Abbasi, J.W. Evans, I.S. Abramson, AIChE J. 29 (1983) 617.
[40] T.E. Springer, T.A. Zawodzinski, S. Gottefeld, J. Electrochem. Soc. 138 (1991) 2334.